In Situ Generated H_2 Bubble-Engaged Assembly: A One-Step Approach for Shape-Controlled Growth of Fe Nanostructures

Guoxiu Tong,[†] Jianguo Guan,*[,†] Zhidong Xiao,[‡] Fangzhi Mou,[†] Wei Wang,[†] and Gongqin Yan[†]

State Key Laboratory of Advanced Technology for Materials Synthesis and Processing, Wuhan University of Technology, No. 122, Luoshi Road, Wuhan 430070, P.R. China, and Department of Chemistry, College of Science, Institute of Chemical Biology, HuaZhong Agricultural University, Wuhan 430070, P.R. China

Received January 27, 2008. Revised Manuscript Received March 7, 2008

The current work describes a simple and convenient approach that allowed for the facile synthesis of Fe nanostructures with morphologies varied from novel solid nanofibers, to nanotubes, and even to hollow nanospheres without using any surfactants and/or solid templates. The morphologically controlled growth of Fe nanostructures can be realized by reducing iron(II) sulfate heptahydrate with sodium borohydride in a carefully devised kinetically tuned procedure, in which the H_2 bubbles generated in situ in the reaction system directed the growth of Fe nuclei. Kinetic factors such as the concentration of the reducing reagent and the reaction temperature can be easily utilized to tune the formation and growth of Fe nuclei and, therefore, the final morphology of the resultant Fe nanostructures. The iron nanostructures were characterized by field-emission scanning electron microscopy (FE-SEM), X-ray energy dispersive spectroscopy (EDS), X-ray diffraction (XRD), transmission electron microscopy (TEM), and vibrating-sample magnetometer (VSM). The one-step H_2 bubble-engaged assembly approach reported here can be readily explored for fabricating other magnetic metal nanostructures, and the resulting Fe nanostructures are expected to find use in a number of applications involving MR imaging, magnetic drug delivery, nanoscale encapsulation, and so forth.

1. Introduction

Recently, one-dimensional (1D) nanostructures such as wires, rods, belts, and tubes have become the focus of intensive research owing to their unique physical properties and potential applications in nanoscale devices.[1–5] Furthermore, magnetic metal nanostructures, especially magnetic metal nanotubes, have aroused the extensive interest of materials researchers due to their intriguing electronic, optical, mechanical, magnetic, and catalytic properties. Interestingly, these intrinsic properties of metal nanostructures can be tailored by controlling their shape, composition, and crystallinity. Among these parameters, shape control has been proved to be as effective as size-control in fine-tuning the properties and functions of metal nanostructures.

Despite their fundamental and technological importance, the challenge of synthetically and systematically controlling the morphology of metal nanostructures has been met with limited success.[6–8] And, up to now, only a few examples of magnetic metal nanotube fabrication have been reported, such as Ni,[9] Fe,[10] Co,[11] and $Fe_{0.32}Ni_{0.68}$ alloy.[12] Mostly, the fabrication of magnetic metal nanotubes mainly depends on the template technique that involves electroless deposition, electrochemical deposition, pulsed electrodeposition, dc electrodeposition, or hydrogen reduction.[13] Usually, different solid materials, including porous alumina, silica, track-etched membranes,[14] microbial microtubules,[15] and polymer membrane were chosen as templates, and the size of the nanotube could be adjusted by choosing appropriate template and reaction conditions.[16] However, the complicated multisteps (including removal of the template) and unfavorable harsh reaction conditions (e.g., imperative annealing step at

* To whom correspondence should be addressed. E-mail: guanjg@whut.edu.cn. Tel: 86-27-87218832. Fax: 86-27-87879468.
[†] Wuhan University of Technology.
[‡] HuaZhong Agricultural University.

(1) Xia, Y. N.; Yang, P. D.; Sun, Y. G.; Wu, Y. Y.; Mayers, B.; Gates, B.; Yin, Y. D.; Kim, F.; Yan, H. Q. *Adv. Mater.* **2003**, *15*, 353.
(2) Puntes, V. F.; Krishnan, K. M.; Alivisatos, A. P. *Science* **2001**, *291*, 2115.
(3) Fang, X.; Bando, Y.; Ye, C.; Shen, G.; Golberg, D. *J. Phys. Chem. C* **2007**, *111*, 8469.
(4) Rout, C. S.; Govindaraj, A.; Rao, C. N. R. *J. Mater. Chem.* **2006**, *16*, 3936.
(5) Li, L.; Yang, Y. W.; Huang, X. H.; Li, G. H.; Ang, R.; Zhang, L. D. *Appl. Phys. Lett.* **2006**, *88*, 103119-1.
(6) Jia, F. L.; Zhang, L. Z.; Shang, X. Y.; Yang, Y. *Adv. Mater.* **2008**, *20*, 1050.
(7) Zhang, Z. T.; Blom, D. A.; Gai, Z.; Thompson, J. R.; Shen, J.; Dai, S. *J. Am. Chem. Soc.* **2003**, *125*, 7528.
(8) Jo, C.; Lee, J. I.; Jang, Y. *Chem. Mater.* **2005**, *17*, 2667.
(9) Tao, F. F.; Guan, M. Y.; Jiang, Y.; Zhu, J. M.; Xu, Z.; Xue, Z. L. *Adv. Mater.* **2006**, *18*, 2161.
(10) Cao, H. Q.; Wang, L. D.; Qiu, Y.; Wu, Q. Z.; Wang, G. Z.; Zhang, L.; Liu, X. W. *ChemPhysChem* **2006**, *7*, 1500.
(11) Nielsch, K.; Castano, F. J.; Ross, C. A.; Krishnan, R. *J. Appl. Phys.* **2005**, *98*, 034318-1.
(12) Xue, S. H.; Cao, C. B.; Wang, D. Z.; Zhu, H. S. *Nanotechnology* **2005**, *16*, 1495.
(13) Sui, Y. C.; Skomski, R.; Sorge, K. D.; Sellmayer, D. *J. Appl. Phys. Lett.* **2004**, *84*, 1525.
(14) Tourillon, G.; Pontonnier, L.; Levy, J. P.; Langlais, V. *Electrochem Solid-State Lett.* **2000**, *3*, 20.
(15) Mogul, R.; Getz Kelly, J. J.; Cable, M. L.; Hebard, A. F. *Mater. Lett.* **2006**, *60*, 19.
(16) Fukunaka, Y.; Motoyama, M.; Konishi, Y.; Ishii, R. *Electrochem. Solid-State Lett.* **2006**, *9*, C62.

10.1021/cm800269k CCC: $40.75
Published on Web 04/25/2008

elevated temperatures in air or selective etching in an appropriate solvent) are unavoidable disadvantages of the conventional template approach, which limits its extensive application.

The low-temperature solution-phase method has the potential to process metals into nanostructures with a range of well-defined morphologies and large scale. Successful synthesis of some particular nanostructures including nanobelts,[17] nanotube,[18] and three-dimensional hierarchical nanoarchitectures,[19] had been accomplished through accurate controlling the experimental condition such as pH value, heating temperature, pressure, and reaction time. Since two or more ingredients in the solution can be fully mixed, this approach is also beneficial to synthesize complex oxides with high homogeneity. Most importantly, this solution-phase synthesis can easily tune the morphological features of resultant nanostructures, because it is facile to kinetically control the nucleation and growth rate of crystals in the dispersion system by choosing appropriate reaction conditions such as template, external applied field, reaction temperature, concentration, and so forth. This method of reducing iron(III) salts by borohydride derivatives in ambient temperature has been widely used to synthesize iron-containing and/or iron nanoparticles, nanowires, and nanonecklaces;[20–24] however, to best of our knowledge, the hollow nanoshperes and nanotubes have not been reported so far.

Here, we demonstrated a simple and convenient approach that allowed for the facile fabrication of Fe nanostructures with morphologies of solid nanofibers, nanotubes, and even hollow nanospheres in absence of any surfactants and/or solid templates. Compared to the reported literature,[20,21] we used the same reducing reagent of sodium borohydride but different starting substance of Fe^{2+} ion and carefully devised the kinetic factors such as the concentration of the reducing agent and the reaction temperature to achieve the morphologically controlled growth of various nanostructures. In this reaction, the H_2 bubbles generated in situ under magnetic stirring directed the assembly of Fe nuclei and easily tune the final morphology of the resultant Fe nanostructures. The one-step in situ generated H_2 bubble-engaged assembly approach depicted here can be readily explored for fabricating other magnetic metal nanostructures, and the resulting Fe nanostructures are expected to find use in a number of applications that involved MR imaging, magnetic drug delivery, nanoscale encapsulation, and so forth.

(17) Liu, Z. P.; Li, S.; Yang, Y.; Peng, S.; Hu, Z. K.; Qian, Y. T. *Adv. Mater.* **2003**, *15*, 1946.
(18) Deng, H.; Wang, J. W.; Peng, Q.; Wang, X.; Li, Y. D. *Chem. Eur. J.* **2005**, *11*, 6519.
(19) Ding, Y. S.; Shen, X. F.; Gomez, S.; Hong, L.; Aindow, M.; Suib, S. L. *Adv. Funct. Mater.* **2006**, *16*, 549.
(20) Lu, L. R.; Ai, Z. H.; Li, J. P.; Zheng, Z.; Li, Q.; Zhang, L. Z. *Cryst. Growth Des.* **2007**, *7*, 459.
(21) Li, X. Q.; Zhang, W. X. *Langmuir* **2006**, *22*, 4638.
(22) Kanel, S. R.; Manning, B.; Charlet, L.; Choi, H. *Environ. Sci. Technol.* **2005**, *39*, 1291.
(23) Giasuddin, A. B. M.; Kanel, S. R.; Choi, H. *Environ. Sci. Technol.* **2007**, *41*, 2022.
(24) Phenrat, T.; Saleh, N.; Sirk, K.; Tilton, R. D.; Lowry, G. V. *Environ. Sci. Technol.* **2007**, *41*, 284.

2. Experimental Section

All reagents, such as iron(II) sulfate heptahydrate ($FeSO_4 \cdot 7H_2O$, AR) and sodium borohydride ($NaBH_4$, AR), were obtained from commercial suppliers and were used without any further purification. Deionized water (10 MΩ·cm) was used in the described reactions and for cleaning the glassware.

Into 200.0 mL of 0.050 M $FeSO_4$ solution in a reaction flask, 100.0 mL of 1.20 M $NaBH_4$ solution was added while the solution was vigorously stirred with a magnetic bar. Note that the reaction system's temperature was precisely controlled at 60 °C using an attached heater, and the rotation rate was maintained about 1200 rpm. After the vigorous magnetic stirring lasted 30 min, the resulting black precipitates were separated, washed several times with deionized water and ethanol, and then dried in vacuum at 40 °C for 24 h to obtain the as-synthesized product of the Fe nanostructure.

The Fe nanostructures with different morphologies were available by changing the concentration of $NaBH_4$ solution and the reaction temperature, respectively.

The morphology of the as-prepared samples was observed by a Hitachi S-4800 field-emission scanning electron microscope (FE-SEM) at an acceleration voltage of 5.0 kV. The phase analyses of the samples were performed by X-ray diffraction (XRD) on a D/MAX-RB diffractometer, using Cu Kα radiation with 2θ from 35° to 90°. The element composition of the samples was characterized by a Horbia EX-250 X-ray energy dispersive spectrometer (EDS) operated at 20.0 kV, associated with FE-SEM. Transmission electron microscopy (TEM) images and the corresponding selected-area electron diffraction (SAED) pattern were captured on the JEM-100CXΠ instrument at an acceleration voltage of 150 kV. The static magnetic properties were measured by a model 4HF vibrating-sample magnetometer (VSM, ADE Co. Ltd., U.S.A.) at room temperature.

3. Results and Discussion

Generally, the reaction temperature and the concentration of the precursor played important roles in determining the morphology of the product. To find the optimal synthetic parameters for generating hollow iron nanostructures, especially nanotubes, we systematically varied the two factors to investigate their influence on the synthesis of specific nanostructure. Figure 1a,b shows that at a relatively lower temperature of 20−35 °C, the products obtained with high yield are not nanotubes but novel chain-like iron nanofibers with diameters of 60−120 nm and lengths of up to several micrometers and with a relatively smooth surface characteristic. In our protocol, the shapes of the resultant iron nanostructures can be readily controlled simply by changing the reaction temperature with all other experimental parameters kept unchanged. As compared to the sample prepared at 20−35 °C, an increase in the temperature (e.g., to 60 °C, Figure 1 c,d) led to the formation of open-ended iron nanotubes with wall thickness of 20−40 nm, inner diameter of about 60−120 nm, and length of up to several hundreds of nanometers as well as relatively rough surface features. Moreover, upon further elevating the reaction temperature (e.g., to 100 °C, Figure 1 e,f), a large number of hollow spheres with diameter in the range of 50−200 nm were obtained; in addition, chain-like hollow spheres can also be observed. From some fragmentized hollow spheres, we can determine their shell thickness is about 20 nm.

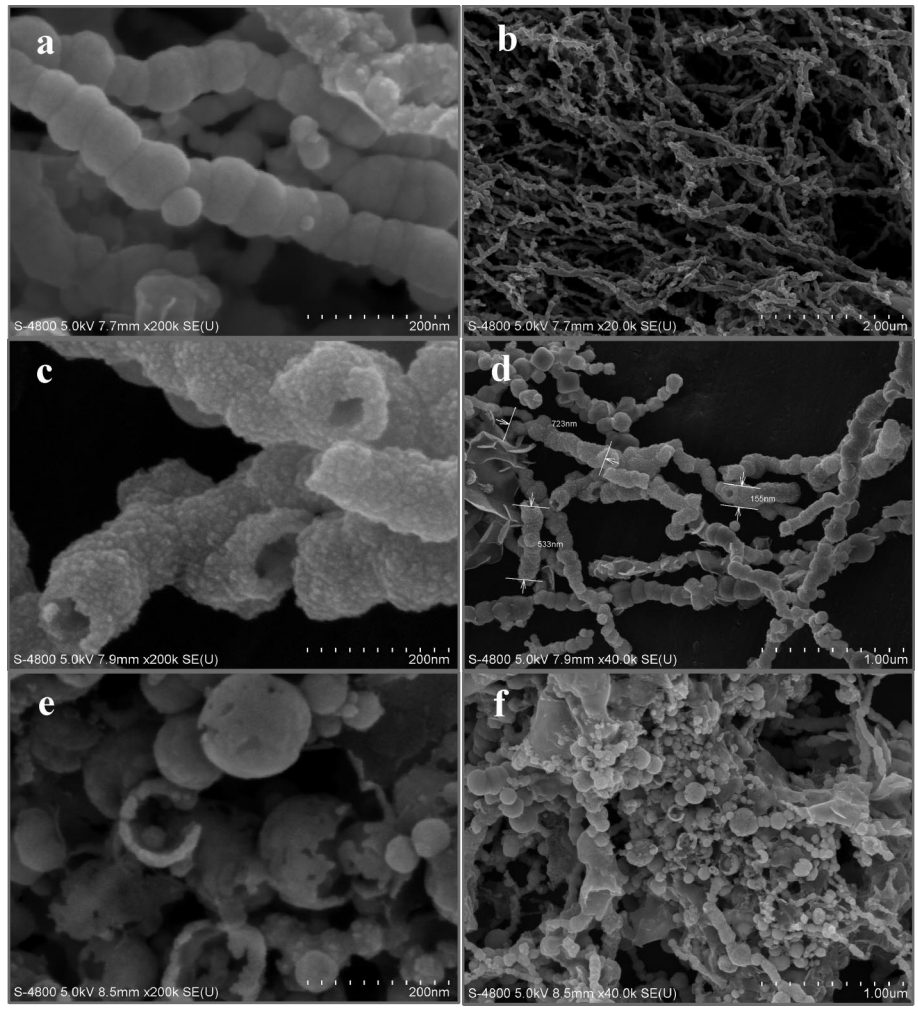

Figure 1. FE-SEM images of the as-synthesized products obtained at various reaction temperatures of (a, b) 20−35 °C, (c, d) 60 °C, and (e, f) 100 °C.

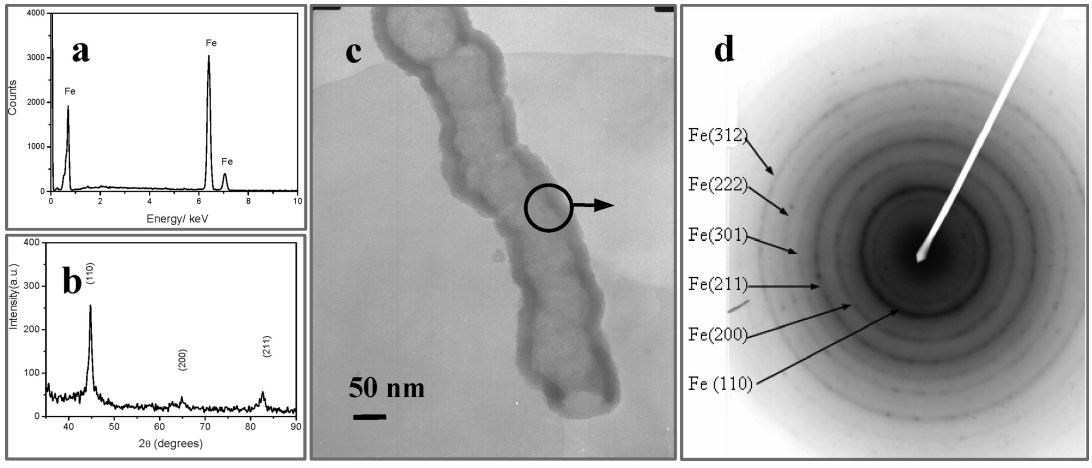

Figure 2. (a) EDS spectrum and (b) XRD pattern taken from the as-synthesized products obtained at 60 °C. (c) TEM image and (d) the corresponding SAED pattern of a typical Fe nanotube.

The composition and the phase structures of the resultant materials are clearly characterized by the EDS spectrum (Figure 2a) and XRD pattern (Figure 2b). EDS analysis on the as-prepared products indicates the existence of only Fe (Figure 2a). From the XRD pattern in Figure 2b, all the peaks in the range of $35° < 2\theta < 90°$ can be indexed as (110), (200), and (211) directions of body-centered cubic (bcc) α-Fe, consistent with the reported data (JCPDS card no. 06-0696). No characteristic peaks of impurities, such as iron oxide or hydroxide, are detected. Both the EDS and the XRD analysis demonstrate that the pure metallic iron products have been obtained and the iron nanostructures are very stable under ambient conditions. Figure 2c shows a typical Fe nanotube obtained at 60 °C with inner diameters of about 100 nm, uniform wall thickness of about 30 nm, and obvious open ends. Weak, diffuse rings in the SAED pattern, shown

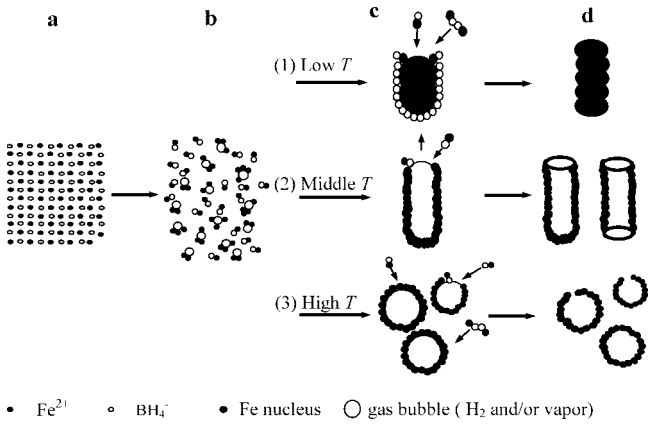

Figure 3. Schematic illustration of the experimental procedure that generates Fe nanofiber, nanotube, and hollow nanospheres: (a) $FeSO_4$ solution; (c) Fe nucleus generated through the reduction of Fe^{2+} by BH_4^-; (c) Fe nucleus congregated on the surfaces of the H_2 bubbles in situ generated and undergone a complex assembly under different temperature conditions; and (d) Fe nanostructures with final morphologies ranging from solid nanofibers, to nanotubes, and even to hollow nanospheres.

in the Figure 2d, suggest that the nanotubes are polycrystalline, and all the face intervals calculated from the diffraction rings (Figure 2d) exactly correspond to the relevant crystal faces of α-Fe.

Figure 3 illustrates the possible steps involved in the generation of various iron nanostructures just via alternating the reaction temperatures. Clearly, not any templates or surfactants are added into the reaction system, and the iron nanostructures are formed by reduction, nucleation, growth, and assembly in a multiphase dispersion system, in which there exists a possible chemical reaction process described as follows:

$$BH_4^- + 2Fe^{2+} + 4H_2O \rightarrow 2Fe\downarrow + B(OH)_4^- + 2H_2\uparrow + 4H^+ \quad (1)$$

$$BH_4^- + H_3O^+ + 2H_2O \rightarrow H_3BO_3 + 4H_2\uparrow \quad (2)$$

$$BH_4^- + 4H_2O \rightarrow B(OH)_4^- + 4H_2\uparrow \quad (3)$$

At the initial stage of the reaction, the Fe nuclei in combination with H_2 bubbles are generated through the reduction of Fe^{2+} ions by BH_4^-, and the majority of Fe nuclei grow into nanocrystals and then congregate into nanoparticles (Figures 3 a,b). H_2 bubbles generated in situ during the reduction reaction play a key role in the formation of different Fe nanostructures. In other words, the morphologies of the products are highly dependent on the size, the number, and the floating rate of H_2 bubbles in the dispersion system. In addition, coagulation of small size H_2 bubbles upon collisions in the dispersion system is also expected to generate bigger H_2 bubbles,[25] which rely on the number of H_2 bubbles generated in situ and the kinetic energy of each H_2 bubble.

No hollow structures but the novel chain-like solid nanofibers are found at the lower temperature of approximately 20 °C. A possible reason is that lower temperature greatly slows down the reduction reaction rate and, therefore, slows down the releasing rate of H_2 gas bubbles and decreases the size of H_2 bubbles, resulting in the bigger surface tension between the gas−solid interfaces and counterworking the agglomeration of iron nuclei on the surface of the H_2 bubbles. In addition, the growth and nucleation rates of Fe nuclei are small at the low temperature, but the growth rate of Fe nuclei is bigger than the nucleation rate of Fe nuclei, which allow more Fe nuclei to deposit not on the surface of H_2 bubbles but around the Fe nuclei, making for the formation of solid Fe nanofibers as shown in Figure 3c(1).

Increasing the reaction temperature to 60 °C will accelerate the reduction reaction and augment the number, size, and floating rate of H_2 bubbles, leading to the formation of nanosized continuous cylinder-shaped gasflow by self-alignment of H_2 bubbles (shown in Figure 3c(2)). At the high temperature, the nucleation and growth rates of Fe nuclei rise; however, the former rate rises much faster than the latter one. Therefore, Fe nuclei encompassing the cylinder-shaped gasflow quickly agglomerate on the surface of the H_2 gasflow by self-organization, forming nanotubes to lower their surface energy. According to the equation $PV/T = nR$, it can be seen that the volume (V) of H_2 bubbles increases with elevating temperature (T) and decreasing intensity of pressure (P). When floating to the solution surface, the H_2 bubbles break open due to the diminishing pressure, resulting in the formation of the open-ended nanotubes (Figure 3c(2)).

Further elevating the temperature to the boiling point of water, large amounts of gas bubbles including both H_2 and vapor generated robustly in the solution will break the stable cylinder-shaped gasflow, providing the sphere template for the formation of Fe hollow nanospheres. A large amount of the hollow nanospheres break up with the swelling gas bubbles in the dispersion system (Figure 3C(3)), resulting in the final morphologies shown in Figure 1 e,f.

Altering the concentration of sodium borohydride, while fixing the reaction temperature at 60 °C and time for 30 min, will also easily tune the morphologies of Fe nanostructures. As shown in Figure 4, increasing the concentration of $NaBH_4$ solution from 0.60 to 1.20 M will hence not only make the surface morphologies of the Fe nanofiber and nanotube smoother but also increase the wall thickness of Fe nanotubes. From the images, we can clearly discern that both nanofibers and nanotubes formed by addition of higher concentration $NaBH_4$ solution are composed of quantities of smaller uniformity nanoparticles with size of ∼15 nm.

In the present method, changing the concentration of reduction agent provides different driving forces for the nucleation and growth of iron nuclei. On one hand, the size and number of H_2 bubbles generated in each condition will change dramatically. On the other hand, the higher the concentration of the added $NaBH_4$, the faster the reduction rate of Fe^{2+} in the reaction system. As a result, the increase of the nucleation rate and the number of Fe nuclei lead to formation of smaller nanocrystals and nanotubes with thicker wall thickness, which can kinetically tune the shapes of the resultants.

The magnetic properties of 1D nanomaterials are believed to be highly dependent on the structure, morphology, and geometry of the materials, such as the diameter and aspect ratio. Figure 5a exhibits the hysteresis loops of iron nanofibers with rough surface morphology and incompact structure obtained by addition of 0.60 M $NaBH_4$ solution. The saturation magnetization (M_s), remanent magnetization (M_r),

(25) Yoon, S. M.; Choi, H. C. *Curr. Appl. Phys.* **2006**, *6*, 747.

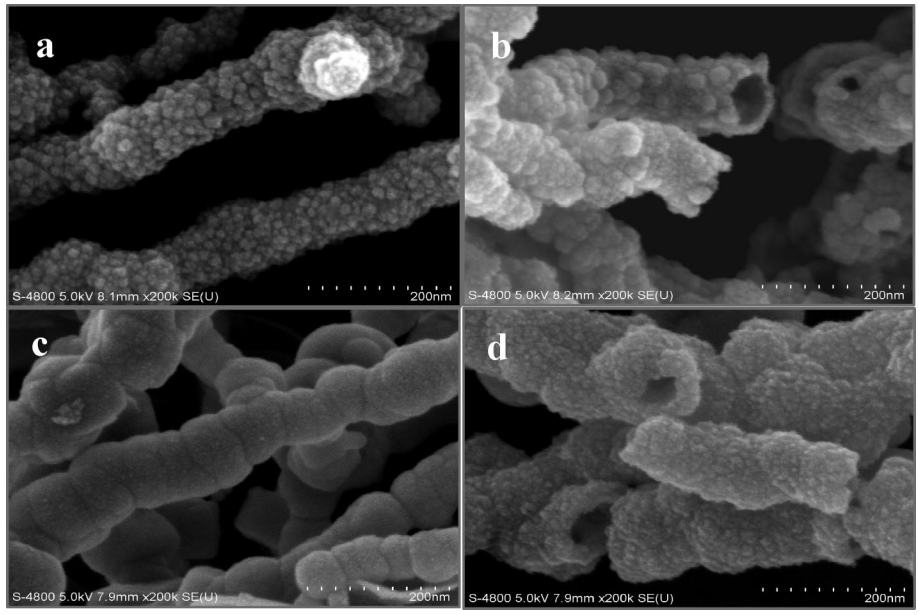

Figure 4. SEM images of two samples obtained with different conditions: (a, b) addition of 0.60 M of $NaBH_4$ solution as reduction agent at 60 °C; (c, d) addition of 1.20 M of $NaBH_4$ solution as reduction agent at 60 °C.

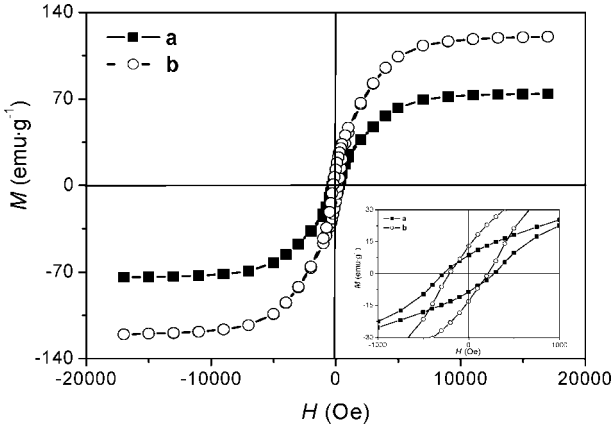

Figure 5. Magnetic hysteresis loops of the samples obtained with the additions of different concentrations of reduction agent: (a) 0.60 M $NaBH_4$ solution; (b) 1.20 M $NaBH_4$.

and coercivity (H_c) values are, respectively, approximately 74.26 emu·g^{-1}, 8.59 emu·g^{-1}, and 280.03 Oe. The hysteresis loop (Figure 5b) of Fe nanotubes with smooth surface morphology, compact chain-like structures obtained by addition of 1.20 M of $NaBH_4$ show a ferromagnetic behavior with M_s, M_r, and H_c values of approximately 120.4 emu·g^{-1}, 12.9 emu·g^{-1}, and 212.9 Oe, respectively. Thus, the above results indicate that the as-synthesized Fe nanofibers exhibit a remarkably enhanced coercivity by comparison with those of bulk Fe (around 2.0 Oe),[26] which may be attributed to their 1D structures and very big aspect ratio (~30). Meanwhile, these results manifest that Fe nanotubes with smooth surface morphology and compact structure have higher M_s, M_r, but lower H_c values than those of Fe nanofibers with coarse surface morphology and incompact structure. This behavior can be related to both the structure of the nanotubes and the surface effect. For the nanotubes with the compact structure, there exist stronger interactions among the nanoparticles, resulting in a higher saturation magnetization (M_s). However, for the nanofibers with rough surface morphology, there is a bigger surface anisotropy,[27] which brings on higher coercivity (H_c) values.

4. Conclusion

In summary, the facile synthesis of Fe nanostructures with morphologies varied from solid nanofibers to nanotubes and even to hollow nanospheres can be achieved via a simple and convenient one-step bubble-engaged assembly approach without using any surfactants and/or solid templates. The shape-controlled growth of Fe nanostructures can be realized by reducing iron(II) sulfate heptahydrate with sodium borohydride in a carefully devised kinetically tuned process, in which the H_2 bubbles generated in situ in the reaction system directed the growth of Fe nuclei under magnetic stirring. Kinetic factors such as the concentration of the reducing agent and the reaction temperature can be easily utilized to tune the formation and growth of Fe nuclei and therefore to tailor the final morphology of the resultant Fe nanostructures. Further works in improving the uniformity of the resultant ferromagnetic iron nanostructures are currently undertaken by us. We believe the one-step bubble-engaged directing reduction reaction approach reported here can be readily extended to synthesize other magnetic metal nanostructures, and the resulting Fe nanostructures are expected to find use in number of applications that involve MR imaging, magnetic drug delivery, nanoscale encapsulation, and so forth.

Acknowledgment. This work was supported by National High-Technology Research and Development Program of China (No. 2006AA03A209), New Century Excellent Talents (No. NCET-05-0660), from the Ministry of Education and Young Teachers from Fok Ying Tung Education Foundation (No. 101049).

CM800269K

(26) Tong, G. X.; Wang, W.; Guan, J. G.; Zhang, Q. J. *J. Inorg. Mater.* **2006**, *21*, 1461.

(27) Tofail, S. A. M.; Rahman, Z. I.; Rahman, A. M.; Mahmood, R. K. U. *Monatsh. Chem.* **2002**, *133*, 859.